PERGAMON

International Journal of Heat and Mass Transfer 43 (2000) 1079–1088

International Journal of HEAT and MASS TRANSFER

www.elsevier.com/locate/ijhmt

Acoustic wave prediction in flowing steam–water two-phase mixture

Jinliang Xu[a,*], Tingkuan Chen[b]

[a]Hemispheric Center for Environmental Technology, Florida International University, 10555 W. Flagler, Eas 2100, Miami, FL 33174, USA

[b]State Key Laboratory on Multiphase Flow, Xi'an Jiaotong University, Xi'an, Shaanxi Province 710049, People's Republic of China

Received 23 February 1999; received in revised form 15 June 1999

Abstract

The transient two-fluid model has been used to develop a general relation for acoustic waves with steam–water two-phase mixture in one-dimensional flowing system. The analysis is valid in principle over the whole void fraction region. Both the mechanical and thermal nonequilibrium are considered. The vapor–liquid interface heat flux is derived from the one dimensional Fourier heat conduction equation to evaluate the interphase evaporation or condensation rate. Calculations are performed for pressures from 0.07 to 16.0 MPa, void fractions from 0.0 to 1.0. Higher frequency limit of sonic velocities are only relied on the pressures and void fractions, and are insensitive to the bubble radius, tube diameter, and the velocity difference between the two phases. The predicted sonic velocities are compared with some experimental data for low pressures. Good agreement has been achieved between the predictions and the experimental data.

1. Introduction

The proper treatment of several nuclear reactor safety problems requires a knowledge of pressure wave propagation in a single-component, two-phase mixture. These include the analysis of choked flows after a postulated break of hot or cold leg of pressurized water reactor and the prediction of the onset of flow instability in parallel boiling channels.

Moody [1] developed a simple acoustic wave model for bubbly flow and annular flow, and established a relationship between sonic velocity and two-phase critical flow. He assumed that no evaporation or condensation will occur when pressure wave is travelling. Similar model was developed by Darcy [2]. Mecredy and Hamilton [3] used the two-fluid model to predict the pressure wave propagation in vapor–liquid flow in detail. However, the analysis contained the important assumption that the evaporation or condensation was governed by kinetic theory. In consequence, the predicted sonic velocities were found to depend strongly on the assumed accommodation coefficients for molecular transfer. Since these coefficients are unknown functions of pressure, temperature and liquid cleanliness, etc., their results implied that sonic velocities and attenuation could never be confidently predicted for a vapour–liquid system.

In recent years, the two-fluid model applied in determining the pressure wave propagation characteristics mainly concerns the pressure wave propagation in low-pressure air–water two-component bubbly flow or annular flow regime [4–6]. For instance, Chung [7] calculated the sonic velocity versus angular frequency from the concept of bubble compressibility in a two-

* Corresponding author. Fax: +1-305-348-1097.
E-mail address: jl_xu@hotmail.com (J. Xu).

0017-9310/00/$ - see front matter
PII: S0017-9310(99)00213-6

Nomenclature

a	Sonic velocity, m/s
a_G	Sonic velocity of saturated vapor, m/s
a_L	Sonic velocity of saturated liquid, m/s
a_I	Interfacial area per unit mixture volume, m^2/m^3
D	Tube inside diameter, m
D_L	Liquid thermal diffusivity, m^2/s
f_I	Interfacial friction coefficient
h_{GL}	Evaporation latent heat, J/kg
i	Imaginary number $\sqrt{-1}$
K	Wavenumber
P	Pressure, Pa
q_{LI}	Heat flux from the liquid to the interface, w/m^2
R_b	Bubble radius, m
S	Slip ratio, U_G/U_L
t	Time, s
T	Temperature, K
U	Velocity, m/s
U_r	Relative velocity between the two phases, m/s
x	Distance from the interface, m
$\bar{x}$	Vapor mass fraction
z	Axial location in one-dimensional flow system, m

Greek symbols

Γ	Evaporation or condensation rate, $kg/(m^3s)$
α	Void fraction of gas phase
η	Attenuation coefficient
λ	Thermal conductivity, w/m °C
μ	Viscosity, kg/m s
π	Arc angular
ρ	Density, kg/m^3
τ	Interface shear stress per unit mixture volume, N/m^3
ω	Angular frequency, Hz
ζ	Any parameter

Subscripts

G	Vapor phase
L	Liquid phase
GI	Vapor phase close to the interface
LI	Liquid phase close to the interface
o	Value of undisturbed flow
sat	Saturated condition
B	Bubbles

component bubbly flow regime. He also extended such a model to predict the sonic velocity of a vapor–liquid system [8].

Compression wave propagation was studied through opening the valve abruptly, while rarefaction wave propagation was investigated through suddenly introducing gas or steam into the flowing two-phase mixture [9–11]. Such experiments were conducted under the condition of either low void fraction, or high void fraction in low pressures.

Let us consider the safety problems related to the loss of coolant accident on the hot or cold leg of the pressurized water reactor. The two-phase critical flow, and the pressure pulse travelling in the reactor core system are mainly governed by the degree at which the two-phase system is relaxed on the mechanical and thermal respects in a variable pressure and void fraction field. However, to authors' knowledge, up to now, not any theoretical model or correlation can calculate the sonic velocities over the whole pressure and void fraction (flow pattern) ranges. This is the main objective of the present job.

A general relation for acoustic waves in a flowing vapor–liquid system was developed. Much attention has been paid to the mechanical and thermal nonequilibrium. Bubbly flow is assumed to exist if void fraction is less than 0.25. We assume that small bubbles may coalescence to form churn flow at void fraction larger than 0.25. Further increasing the void fraction to be larger than 0.8 will result in the churn flow absorbing all smaller bubbles to form annular flow. Different correlations are used to predict the interfacial area and interfacial drag force per unit mixture volume for different flow regimes.

2. Mathematical models

The present theory depends mainly upon the following assumptions:

- The flow system is one-dimensional;
- Before the travelling of the pressure wave front the flow is in thermal and mechanical equilibrium. However, the flow is in thermal and mechanical nonequilibrium when the pressure wave is travelling;
- Flow pattern transitions are assumed to occur at certain void fractions.

We consider the motion of small amplitude monochromatic waves of frequency ω, wave number K, travelling along the duct axial location z. In the disturbed flow, oscillations in the primary variables are

given by

$$\zeta = \zeta_o + \Delta\zeta \exp[i(\omega t - Kz)] \tag{1}$$

General equations of one-dimensional two-fluid model for the conservation of mass and momentum are coming from [12], neglecting the friction pressure loss between the wall surface and the two phases.

$$\rho_G \frac{\partial \alpha}{\partial t} + \alpha \frac{\partial \rho_G}{\partial t} + \rho_G U_G \frac{\partial \alpha}{\partial z} + \alpha U_G \frac{\partial \rho_G}{\partial z} + \alpha \rho_G \frac{\partial U_G}{\partial z} = \Gamma_G \tag{2}$$

$$-\rho_L \frac{\partial \alpha}{\partial t} + (1-\alpha)\frac{\partial \rho_L}{\partial t} - \rho_L U_L \frac{\partial \alpha}{\partial z} + (1-\alpha) U_L \frac{\partial \rho_L}{\partial z} + (1-\alpha)\rho_L \frac{\partial U_L}{\partial z} = \Gamma_L \tag{3}$$

$$\alpha \rho_G \frac{\partial U_G}{\partial t} + \alpha \rho_G U_G \frac{\partial U_G}{\partial z} + \alpha \frac{\partial P}{\partial z} = (U_{GI} - U_G)\Gamma_G + \tau_{GI} \tag{4}$$

$$(1-\alpha)\rho_L \frac{\partial U_L}{\partial t} + (1-\alpha)\rho_L U_L \frac{\partial U_L}{\partial z} + (1-\alpha)\frac{\partial P}{\partial z} = (U_{LI} - U_L)\Gamma_L + \tau_{LI} \tag{5}$$

The two-phase energy equations are not used here. This is useful to simplify the derivation of the general wave number K equation. In fact, considering the mass transfer of the interface evaporation, or condensation rate in mass equations reflects the energy exchange between the two phases. In addition, we shall note that $\Gamma_G + \Gamma_L = 0$, $\tau_{GI} + \tau_{LI} = 0$. The differential terms of $(\partial\rho/\partial t)$ and $(\partial\rho/\partial z)$ for phase G and phase L can be replaced by the differential terms of $(\partial P/\partial t)$ and $(\partial P/\partial z)$ through introducing the single phase sound speeds for both phases:

$$\frac{\partial \rho_G}{\partial t} = \frac{\partial \rho_G}{\partial P}\frac{\partial P}{\partial t} = \frac{1}{a_G^2}\frac{\partial P}{\partial t} \tag{6}$$

$$\frac{\partial \rho_L}{\partial t} = \frac{\partial \rho_L}{\partial P}\frac{\partial P}{\partial t} = \frac{1}{a_L^2}\frac{\partial P}{\partial t} \tag{7}$$

$$\frac{\partial \rho_G}{\partial z} = \frac{\partial \rho_G}{\partial P}\frac{\partial P}{\partial z} = \frac{1}{a_G^2}\frac{\partial P}{\partial z} \tag{8}$$

$$\frac{\partial \rho_L}{\partial z} = \frac{\partial \rho_L}{\partial P}\frac{\partial P}{\partial z} = \frac{1}{a_L^2}\frac{\partial P}{\partial z} \tag{9}$$

where a_L and a_G are sound speeds of saturated water and steam, which are determined by [13] in this study. Therefore Eqs. (2)–(5) are modified to be

$$\rho_G \frac{\partial \alpha}{\partial t} + \alpha a_G^{-2}\frac{\partial P}{\partial t} + \rho_G U_G \frac{\partial \alpha}{\partial z} + \alpha U_G a_G^{-2}\frac{\partial P}{\partial z} + \alpha \rho_G \frac{\partial U_G}{\partial z} = \Gamma_G \tag{10}$$

$$-\rho_L \frac{\partial \alpha}{\partial t} + (1-\alpha)a_L^{-2}\frac{\partial P}{\partial t} - \rho_L U_L \frac{\partial \alpha}{\partial z} + (1-\alpha)U_L a_L^{-2}\frac{\partial P}{\partial z} + (1-\alpha)\rho_L \frac{\partial U_L}{\partial z} = \Gamma_L \tag{11}$$

$$\alpha \rho_G \frac{\partial U_G}{\partial t} + \alpha \rho_G U_G \frac{\partial U_G}{\partial z} + \alpha \frac{\partial P}{\partial z} = (U_{GI} - U_G)\Gamma_G + \tau_{GI} \tag{12}$$

$$(1-\alpha)\rho_L \frac{\partial U_L}{\partial t} + (1-\alpha)\rho_L U_L \frac{\partial U_L}{\partial z} + (1-\alpha)\frac{\partial P}{\partial z} = (U_{LI} - U_L)\Gamma_L + \tau_{LI} \tag{13}$$

Solutions of Eqs. (10)–(13) constitute the matrix $(\alpha, P, U_G, U_L)^T$. We notify that the matrix $(\alpha_o, P_o, U_{G,o}, U_{L,o})^T$ can satisfy Eqs. (10)–(13) before the flow is disturbed. However, when the pressure pulse travels in the flow system,

$$(\alpha, P, U_G, U_L)^T = (\alpha_o, P_o, U_{G,o}, U_{L,o})^T + (\delta\alpha, \delta P, \delta U_G, \delta U_L)^T \exp[i(\omega t - Kz)] \tag{14}$$

can also satisfy Eqs. (10)–(13). Thus the four equations before the flow is disturbed, incorporating another four equations with mechanical and thermal nonequilibrium after the pressure pulse is travelling in the system, consist of eight equations. Simplifying the above eight equations and further determining the interface parameters Γ_G, Γ_L, τ_{GI}, τ_{LI}, U_{GI} and U_{LI}, will eventually result in the wave number K equation.

2.1. Evaporation or condensation rate

The evaporation rates are assumed to be governed by the conduction heat transfer from liquid to the interface. This assumption is useful in bubble growth analysis. Such evaporation rate is

$$\Gamma_G = -\Gamma_L = -\frac{q_{LI} a_I}{h_{GL}} \tag{15}$$

The diffusive heat flux can be calculated by solving the one-dimensional Fourier equation in the liquid close to the interface. At a distance x from the interface, we have

$$\frac{\partial^2 T_L}{\partial x^2} = \frac{1}{D_L}\frac{\partial T_L}{\partial t} \tag{16}$$

subject to the boundary conditions of

$$T_L \to T_o + \delta T_{LI}\exp[i(\omega t - Kz)] \quad \text{as} \quad x \to 0 \tag{17}$$

$$T_L \to T_o \quad \text{as} \quad x \to \infty \tag{18}$$

The solution of Eq. (16) satisfying the above boundary conditions is

$$T_L = T_o + \delta T_{LI}\exp[i(\omega t - Kz - K^* x)] \tag{19}$$

The interface heat flux is simply

$$q_{LI} = -\lambda_L \frac{\partial T_L}{\partial x}_{x=0}$$

$$= \delta T_{LI}\omega^{0.5}\lambda_L D_L^{-0.5}\exp\left[i\left(\omega t - Kz + \frac{\pi}{4}\right)\right] \tag{20}$$

It should be noted that the heat flux leads the driving temperature by 45°.

It is assumed that the vapor phase is saturated corresponding to the system pressure. Because the interface heat transfer coefficient is large, the liquid interface subject to the vapor phase is assumed to have the same temperature of the vapor phase. Based on these, liquid temperature change due to the pressure pulse is $\delta T_{LI} = (dT/dP)_{sat}\delta P$, where $(dT/dP)_{sat}$ is the gradient of temperature versus pressure along the saturated line. The analysis is correct for low frequency of pressure pulse, for instance $\omega < 10^3$ Hz. When the frequency is well above the bubble resonance, for instance $\omega > 10^5$ Hz, further study is expected on the better interface heat and mass transfer model. The vapor and liquid pressures are not equal at such conditions. The present assumptions result in the following interface heat flux correlation.

$$q_{LI} = \omega^{0.5}\lambda_L D_L^{-0.5}\left(\frac{dT}{dP}\right)_{sat}\exp\left(i\frac{\pi}{4}\right)\delta P\exp[i(\omega t - Kz)] \tag{21}$$

and

$$\Gamma_G = -\Gamma_L = -\omega_q h_{GL}^{-1}\delta P\exp[i(\omega t - Kz)] \tag{22}$$

where

$$\omega_q = \omega^{0.5}\lambda_L D_L^{-0.5} a_I\left(\frac{dT}{dP}\right)_{sat}\exp\left(i\frac{\pi}{4}\right) \tag{23}$$

2.2. Interfacial area and interfacial drag force

For small periodic changes in the liquid and vapor system, the interface drag may be expanded in the linear approximation to give

$$\tau_{GI} = -\tau_{LI} = \tau_{GI,o} + \tau'(\delta U_G - \delta U_L)\exp[i(\omega t - Kz)] \tag{24}$$

where

$$\tau' = \frac{\partial \tau_{GI}}{\partial U_G} = -\frac{\partial \tau_{GI}}{\partial U_L} = -\frac{\partial \tau_{LI}}{\partial U_G} = \frac{\partial \tau_{LI}}{\partial U_L} \tag{25}$$

The form of τ_{GI} depends on the flow regime, specific examples are inserted for illustrative calculations given as follows.

2.2.1. Bubbly flow regimes

In bubbly flow regime, assuming a uniform distribution of spherical bubbles of mean radius R_b, we can drive the interfacial area per unit mixture volume as

$$a_I = \frac{3\alpha}{R_b} \tag{26}$$

Wallis [14] obtained an expression of τ_{GI} from the expression for the drag on a single sphere.

$$\tau_{GI} = -\tau_{LI}$$

$$= -\frac{9\alpha\mu_L U_r}{2R_b^2} - \frac{\alpha}{2}\rho_L\frac{1+2\alpha}{1-\alpha}\left(\frac{\partial U_r}{\partial t} + U_G\frac{\partial U_r}{\partial z}\right) \tag{27}$$

The first term is the Stokes viscous drag, and the second term represents the inertia drag due to the virtual mass of the bubble.

According to Eq. (25), we have

$$\tau = -\frac{9\alpha\mu_L}{2R_b^2} - i\frac{\alpha}{2}\frac{1+2\alpha}{1-\alpha}\rho_L(\omega \quad - U_G K) \tag{28}$$

2.2.2. Annular flow regime

In annular flow regime, assuming that the liquid film is distributed uniformly on the tube wall, we can write the interfacial area per unit mixture volume as

$$a_I = \frac{4\sqrt{\alpha}}{D} \tag{29}$$

Wallis [14] proposed an expression of interfacial drag force per unit mixture volume to be

$$\tau_{GI} = -\frac{1}{2}f_I\rho_G a_I U_r^2 \tag{30}$$

$$f_I = 0.005[1 + 75(1-\alpha)] \tag{31}$$

So we have

$$\tau' = -f_I\rho_G a_I U_r \tag{32}$$

2.2.3. Churn flow regime

Through analyzing the minimum distance between bubbles to keep bubbles move freely, Griffith et al. [15] suggested that the coalescence possibility is increased and eventually flow regime transition occurs from bubbly flow to other flow regimes, such as slug flow or churn flow, if void fraction is larger than 0.25. The published experimental data also show that no bubble coalescence occurs in bubbly flow regime if $\alpha < 0.2$, but the void fraction can not exceed 0.3 in bubbly flow [16]. Therefore the present model specifies the critical void fraction at which the bubbles begin to coalescence and eventually induce the churn flow to be 0.25. It should be noted that the above flow pattern transition criteria is a rough estimation. Such transition is complicated for a certain flow system, and depends on the two-phase flow rate, void fraction, fluid properties, flow direction versus gravity, and pipe diameter and so on. However, the above transition estimation based on the void fraction is very useful to simplify the pressure wave analysis, and can give useful information on the sonic velocity and attenuation. In churn flow regime, the interface area and drag force are estimated as a liner relations between the bubbly flow and annular flow versus void fraction.

$$a_{\mathrm{I}} = a_{\mathrm{I},\alpha=0.25} + \frac{(\alpha-0.25)}{(0.8-0.25)}(a_{\mathrm{I},\alpha=0.8} - a_{\mathrm{I},\alpha=0.25}) \tag{33}$$

$$\tau' = \tau'_{\alpha=0.25} + \frac{(\alpha-0.25)}{(0.8-0.25)}(\tau'_{\alpha=0.8} - \tau'_{\alpha=0.25}) \tag{34}$$

It is assumed that the annular flow exists when the void fraction begins to exceed 0.8.

2.2.4. Determination of U_{GI} and U_{LI}

The velocity field is continuous across the interphase boundary, with the interface velocity equal to the bulk velocity of the liquid phase [17],

$$U_{\mathrm{GI}} = U_{\mathrm{LI}} = U_{\mathrm{L}} \tag{35}$$

This is reasonable for separated flows when $(U_{\mathrm{G}}-U_{\mathrm{L}})$ is large. In bubbly flow regime, the interface velocity is close to the gas velocity of U_{G}. However, in this case the large mutual drag force ensures that $U_{\mathrm{G}} \cong U_{\mathrm{L}}$, thus the use of Eq. (35) introduces only a small error.

3. Solution of the present model

To simplify Eqs.(10)–(13), we obtain the following four linear homogeneous equations with four unknown quantities.

$$\begin{aligned}
&\mathrm{i}(\omega - U_{\mathrm{G}}K)\rho_{\mathrm{G}}\delta\alpha + [\mathrm{i}(\omega - U_{\mathrm{G}}K)\alpha a_{\mathrm{G}}^{-2} \\
&\quad + \omega_q h_{\mathrm{GL}}^{-1}]\delta P - \mathrm{i}\alpha K\rho_{\mathrm{G}}\delta U_{\mathrm{G}} = 0, \\
&\quad - \mathrm{i}(\omega - U_{\mathrm{L}}K)\rho_{\mathrm{L}}\delta\alpha + [\mathrm{i}(\omega - U_{\mathrm{L}}K)(1-\alpha)a_{\mathrm{L}}^{-2} \\
&\quad - \omega_a h_{\mathrm{GL}}^{-1}]\delta P - \mathrm{i}(1-\alpha)K\rho_{\mathrm{L}}\delta U_{\mathrm{L}} = 0 \\
&[-\mathrm{i}\alpha K + \omega_q h_{\mathrm{GL}}^{-1}(U_{\mathrm{L}} - U_{\mathrm{G}})]\delta P + [\mathrm{i}\alpha\rho_{\mathrm{G}}(\omega \\
&\quad - U_{\mathrm{G}}K) - \tau']\delta U_{\mathrm{G}} + \tau'\delta U_{\mathrm{L}} = 0, \\
&\mathrm{i}(1-\alpha)K\delta P + \tau'\delta U_{\mathrm{G}} + [\mathrm{i}(1-\alpha)\rho_{\mathrm{L}}(\omega \\
&\quad - U_{\mathrm{L}}K) - \tau']\delta U_{\mathrm{L}} = 0
\end{aligned} \tag{36}$$

For a unique solution of the above equations to exist, the determinant of the coefficient matrix must vanish, this implies that

$$\begin{vmatrix}
\mathrm{i}(\omega - KU_{\mathrm{G}})\rho_{\mathrm{G}} & \mathrm{i}(\omega - KU_{\mathrm{G}})\alpha a_{\mathrm{G}}^{-2} + \omega_q h_{\mathrm{GL}}^{-1} & -\mathrm{i}\alpha K\rho_{\mathrm{G}} & 0 \\
-\mathrm{i}(\omega - KU_{\mathrm{L}})\rho_{\mathrm{L}} & \mathrm{i}(1-\alpha)(\omega - U_{\mathrm{L}}K)a_{\mathrm{L}}^{-2} - \omega_q h_{\mathrm{GL}}^{-1} & 0 & -\mathrm{i}(1-\alpha)K\rho_{\mathrm{L}} \\
0 & -\mathrm{i}\alpha K + \omega_q h_{\mathrm{GL}}^{-1}(U_{\mathrm{L}} - U_{\mathrm{G}}) & \mathrm{i}\alpha\rho_{\mathrm{G}}(\omega - U_{\mathrm{G}}K) - \tau' & \tau' \\
0 & -\mathrm{i}(1-\alpha)K & \tau' & \mathrm{i}(1-\alpha)\rho_{\mathrm{L}}(\omega - U_{\mathrm{L}}K) - \tau'
\end{vmatrix} = 0 \tag{37}$$

Then Eq. (37) has four independent solutions of $K_{\mathrm{i}}(\omega)$ corresponding to two 'path waves' advancing with the bulk phase velocity U_{L} and U_{G}, and two 'composite waves' which are a mixture of acoustic and kinematic perturbations. A useful dispersion relation can be made by considering flows at low Mach numbers, U_{G}, $U_{\mathrm{L}} \ll \omega/K$ such that $\omega - U_{\mathrm{G}}K \cong \omega$, $\omega - U_{\mathrm{L}}K \cong \omega$. The composite waves then degenerate into two path waves and two acoustic waves. Multiplying out the determinant in Eq. (37), the wave numbers of the acoustic disturbances can be shown to be roots of the quadratic equation.

$$\{-\alpha(1-\alpha)\rho_L\rho_G\omega[\alpha\rho_L+(1-\alpha)\rho_G]-i\rho_L\rho_G\tau'\}K^2$$
$$+(1-\alpha)\rho_L\rho_G\omega_q h_{GL}^{-1}(U_L-U_G)(\tau'-i\alpha\rho_L\omega)K$$
$$+\alpha(1-\alpha)\rho_L\rho_G\omega^3[(1-\alpha)\rho_G a_L^{-2}+\alpha\rho_L a_G^{-2}]$$
$$+[\alpha\rho_G+(1-\alpha)\rho_L]\omega(\rho_L-\rho_G)\omega_q h_{GL}^{-1}\tau'$$
$$+i\omega^2[\alpha\rho_G+(1-\alpha)\rho_L][\alpha\rho_L a_G^{-2}$$
$$+(1-\alpha)\rho_G a_L^{-2}]\tau'+i\alpha(1-\alpha)\rho_L\rho_G\omega^2\omega_q h_{GL}^{-1}(\rho_G$$
$$-\rho_L)=0 \quad (38)$$

The two roots of the above equation are equal but opposite in sign. One of them represents a wave moving in z direction and the other in the negative direction. The real part of K is then used to obtain the sonic velocity $a=\omega/\mathrm{Re}al(K)$, while the imaginary part of the root equals to η, the wave number attenuation coefficient.

4. Results and discussion

Results of illustrative calculations for two-phase sonic velocities and attenuation coefficients as a function of angular frequency are plotted in Figs. 1–3 for various void fractions at pressure of 16.0 MPa. Calculations at pressure of 16.0 MPa are of interest to the typical pressurized water reactor due to such press-

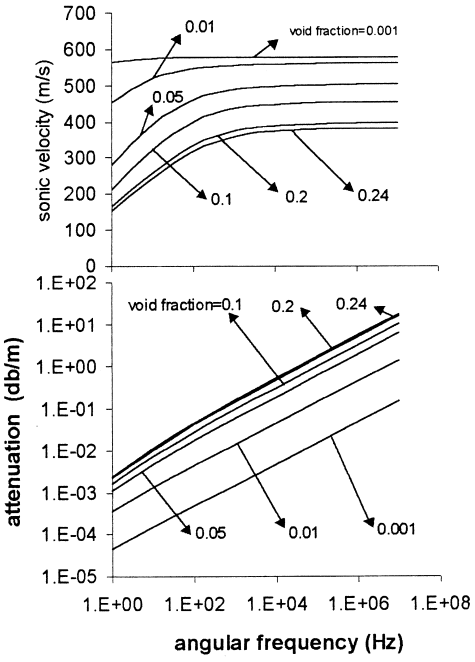

Fig. 1. Sonic velocities and attenuation coefficients versus angular frequencies in bubbly flow regime at P = 16.0 MPa, R_b = 0.5 mm, and U_r = 0.5 m/s.

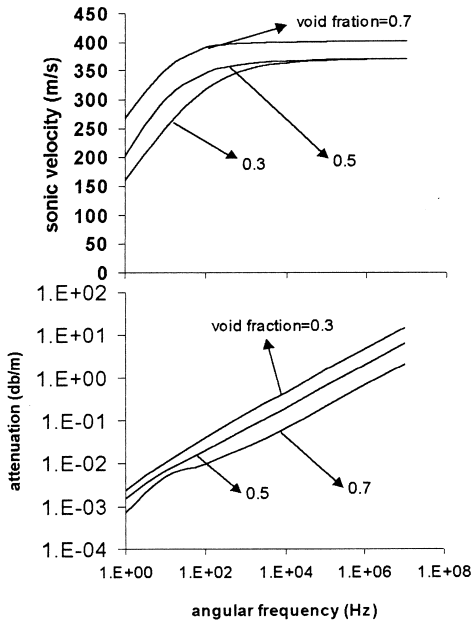

Fig. 2. Sonic velocities and attenuation coefficients versus angular frequencies in churn flow regime at P = 16.0 MPa, U_r = 0.5 m/s, and D = 20.0 mm.

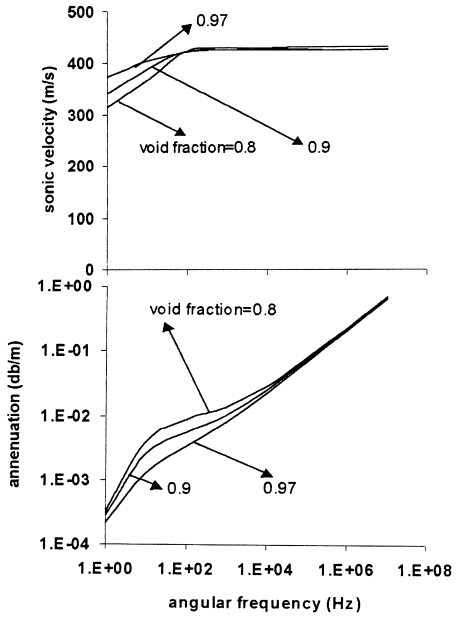

Fig. 3. Sonic velocities and attenuation coefficients versus angular frequencies in annular flow regime at P = 16.0 MPa, U_r = 0.5 m/s and D = 20.0 mm.

ure being nearly equal to the steady state operation pressure. Results are given for bubble radius of 0.5 mm, vapor–liquid relative velocity of 0.5 m/s in a tube of 20.0 mm inside diameter. However, in bubbly flow regime the tube diameter is not required. In annular flow regime, bubble radius is not needed. From these figures, the following conclusions can be drawn.

In any flow regime, sonic velocities increase with increasing angular frequency at low angular frequency ($\omega < 10^3 \sim 10^4$ Hz). Once the frequency reaches the value of $10^3 \sim 10^4$ Hz, the sonic velocity obtains a limit value. At low frequency, more time is provided for the momentum and thermal transport between the phases to make the mixture 'softer' and increase the bubble compressibility, such that lower sonic velocity results. In other words, the lower frequency limit of sonic velocity is close to be governed by mechanical and thermal equilibrium in the mixture. At higher frequencies, for instance $\omega > 10^4$ Hz, less time is provided for the mixture to reach the mechanical and thermal equilibrium, and the mixture becomes 'stiffer', which results in higher sonic velocity. Higher frequency limit of sonic velocity is close to be dominated by the mechanical and thermal nonequilibrium in the mixture.

In bubbly flow regime (see Fig. 1), sonic velocities are sensitive to the variation of the void fractions. Lower sonic velocity results from the increased compressibility of the mixture when the void fraction is increased. The attenuation coefficients rise with increasing void fractions.

In churn flow regime with medium void fractions, sonic velocities and attenuation coefficients as a function of angular frequency are illustrated in Fig. 2. Predictions show that higher frequency limit of sonic velocity versus void fractions has a minimum value. The attenuation coefficients are decreased with increasing the void fraction, which is different from that of bubbly flow.

In annular flow regime, little influence of void fraction on the sonic velocity is found (see Fig. 3). Sonic velocities at different void fractions are very close to those of saturated vapor. For instance, the two-phase sonic velocity at pressure of 8.0 MPa and void fraction of 0.8 is 488 m/s, which is very close to that of the saturated vapor of 486 m/s at the same pressure. Both liquid and vapor phases are continuous phases when the flow is in annular flow regime with vapor flowing in the core and the liquid flowing as a film along the tube wall. The two-phase sonic velocity is very close to that of saturated vapor, which is verified by the experiments, even though some liquid droplets entrained in the gas core are not considered in the present model. Figure 3 also illustrates the insensitive attenuation coefficients versus void fraction in the annular flow regime.

Theoretical curves of sonic velocities versus pressures

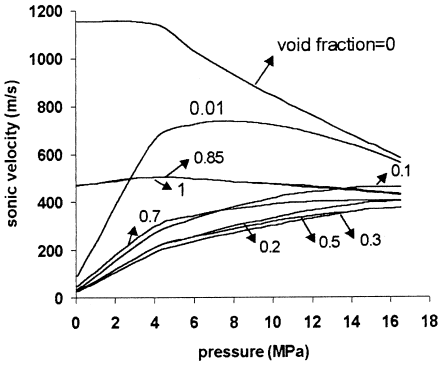

Fig. 4. Effect of pressure on the sonic velocities at different void fractions.

are illustrated in Fig. 4 at different void fractions. Sonic velocities of saturated liquid and vapor are plotted based on the data of Ref. [13]. It is found that the effects of pressure on the sonic velocities are complicated. At the fixed, very low void fractions, for instance $\alpha < 0.01$, with increasing pressures, sonic velocity increases, obtains a maximum value, then decrease. At larger void fractions (bubbly flow or churn flow), sonic velocity is increased with increasing the pressures. Sonic velocity at void fraction of 0.85 is nearly equal to that of saturated vapor.

Based on the present theory, two-phase sonic velocities depend on the pressure, void fraction, angular frequency, vapor–liquid relative velocity ($U_r = U_G - U_L$). Additional information on bubble radius R_b in bubbly flow regime, and tube diameter D in annular flow regime are also required. The angular frequency governs the degree at which the two-phase mixture relaxes on the mechanical and thermal respects. Pressure affects the physical properties.

Bubble radius, tube diameter and the relative velocity difference between the two phases affect the momentum or the mass exchange between the two phases. Figure 5 shows the sonic velocities versus angular frequencies at different void fractions and different bubble radius in bubbly flow regime. Assuming the bubble radius of 1.0 and 0.5 mm only affect the sonic velocities at low angular frequencies, for instance $\omega < 10^3$ Hz. Increasing the bubble radius will decrease the interface area between the two phases and decrease the evaporation or condensation rate, thus result in larger sonic velocities. However, the above conclusion is only valid at low angular frequency. Bubble radius does not influence the higher frequency limit of sonic velocity. This is because the sonic velocities are close to be governed by the mechanical and thermal nonequilibrium at high frequency. In a practical two-phase system, the bubble size is not uniform and shall have a size distribution. However,

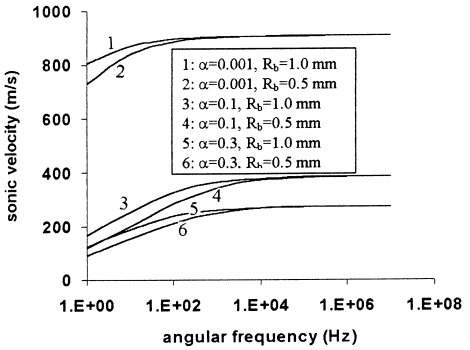

Fig. 5. Effect of bubble radius on the sonic velocity in bubbly and churn flow regime at $P = 8.0$ MPa, $U_r = 0.5$ m/s and $D = 20.0$ mm.

the higher frequency limit of sonic velocity is not depended on such size distribution, which is very helpful for the measurements of the sonic velocities.

Figure 6 gives the effect of pipe diameter on the sonic velocities. Pipe diameter only affects the sonic velocities at low angular frequencies. Review on the effects of velocity difference between the two phases also leads to the same conclusion and the results are not shown in the present paper. Any parameter, which increases the momentum or the mass exchange between the phases, can decrease the sonic velocities at low angular frequencies. However, higher frequency limits of sonic velocities are insensitive to such parameters. Based on the above analysis, the higher frequency limit of sonic velocity is mainly relied on the system pressure and void fraction.

Thermally controlled bubble growth is appropriate for certain growth rates at low frequencies such as $\omega < 10^4$ Hz. At very high angular frequencies, the frequencies are well above the bubble resonance so the vapor and liquid pressure are not equal. The gas phase shall not be saturated corresponding to its pressure. The mixture wavelength is also less than the bubble diameter. Therefore, better model on the evaporation rate between the phases is expected. However, the present calculations show that the higher frequency limits of sonic velocities are insensitive to such evaporation rate models. At very high angular frequency, results from any different bubble growth models shall be close to be 'frozen' due to very less time provided between the phases. The present model is correct for many critical flashing flows.

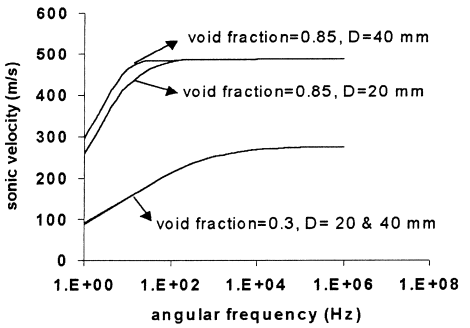

Fig. 6. Effect of pipe diameter on the sonic velocities in annular flow regimes at $P = 8.0$ MPa and $U_r = 0.5$ m/s.

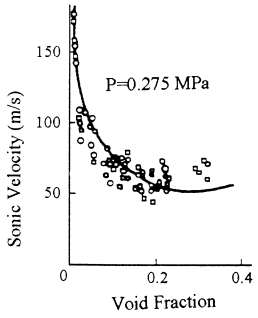

Fig. 7. Comparison of sonic velocity predictions with experimental data [18].

Higher frequency limits of sonic velocities are interesting to the practical engineering applications. Henry [18], England [10] and Karplus [19] measured the two-phase sonic velocity at low pressures. Comparisons of the present predictions with their experimental data are shown in Figs. 7–10. Based on the present study, the higher frequency limit of sonic velocities are attained at $\omega = 10^3 \sim 10^4$ Hz, therefore, calculations in Figs. 7–10 are performed at $\omega = 10^4$ Hz. In bubbly flow, bubble radius is estimated by the classical correlation such as [20]

$$R_b = 0.925\alpha^{0.243}(\sigma/g\Delta\rho)(G/\mu_L)^{0.1} \tag{39}$$

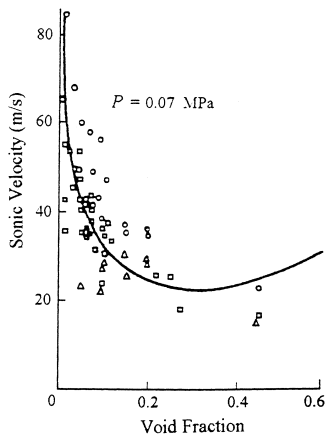

Fig. 8. Comparison of sonic velocity predictions with experimental data [19].

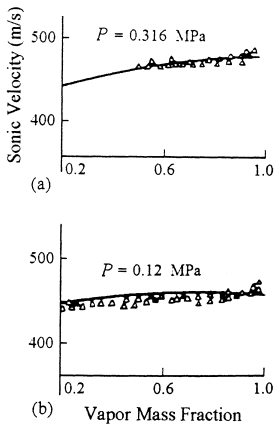

Fig. 9. Comparison of sonic velocity predictions with experimental data [10].

Assuming a liquid velocity, the velocity difference between the two phases is determined as $(S-1)U_L$, where S is the slip ratio. In Fig. 9 void fractions are determined by

$$\alpha = 1/[1 + S\rho_G(1-\overline{x})/(\rho_L\overline{x})] \tag{40}$$

Corresponding to the void fractions, the annular flow exists in Fig. 9. Figure 10 shows the comparison of the present predictions with experimental data obtained by Kaizerman et al. [21] at a pressure of 2.0 MPa. From these four curves, the consistency of the measured values with the theory over the whole range of the phase distribution considered is remarkable.

Critical flow is an important topic in the safety analysis of nuclear power plants. Physically, when critical flow occurs, the signal of pressure variation downstream can not propagate upstream, and critical mass flux can be determined as $G = \bar{\rho}a$. For instance, nuclear power plant thermal hydraulic codes such as, TRAC-PFI, RELAP5 include the sonic velocity model to predict the critical mass flux. However, critical mass flux is predicted poorly due to the accuracy of the sonic velocities. It is clear that the present job will be helpful to improve such calculations.

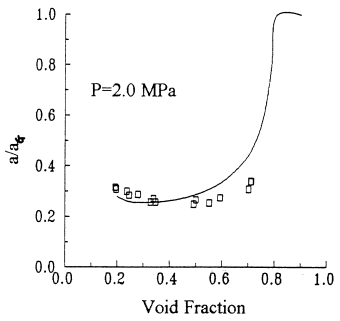

Fig. 10. Comparison of sonic velocity predictions with experimental data [21].

5. Conclusions

1. A wave number K equation is developed in this paper and it can be used to predict the two-phase sonic velocity over a wide range of parameters. Both mechanical and thermal nonequilibrium are considered in the model.
2. In any flow regime, the sonic velocity increases with increasing the frequency at $\omega < 10^3 \sim 10^4$ Hz, and is close to be controlled by the equilibrium. However, higher frequency limit of sonic velocity obtains a limit value, and is close to be governed by the mechanical and thermal nonequilibrium.
3. High frequency limit of sonic velocities are decreased with increasing the void fraction in bubbly flow regime, attain a minimum value in churn flow regime, and are close to those of saturated vapor in annular flow regime.
4. Bubble radius, tube diameter, and the velocity difference between the two phases affect the sonic velocities at low frequencies. However, the sonic velocities are insensitive to the variations of these parameters at high frequencies.
5. The present prediction results match the experimental data very well.

Acknowledgements

The authors would like to thank the Natural Science Foundation of China for the financial support.

References

[1] F.J. Moody, A pressure pulse model for two-phase critical flow and sonic velocity, J. Heat Transfer (1969) 371–384.
[2] D.F. Darcy, On acoustic propagation and critical mass flux in two-phase flow, J. Heat Transfer (1971) 413–421.
[3] R.C. Mecredy, L.J. Hamilton, The effects of nonequilibrium heat, mass and momentum transfer on two-phase sound speed, Int. J. Heat Mass Transfer 15 (1972) 61–72.
[4] L.Y. Cheng, D.A. Drew, R.T. Lahey Jr, An analysis of wave propagation in bubbly two-component, two-phase flow, J. Heat Transfer 107 (1985) 402–408.
[5] A.E. Ruggles, R.T. Lahey Jr, D.A. Drew, H.A. Scarton, An investigation of the propagation of pressure perturbations in bubbly air/water flows, J. Heat Transfer 110 (1988) 494–499.

[6] A.E. Ruggles, R.T. Lahey Jr, D.A. Drew, H.A. Scarton, The relationship between standing waves, pressure pulse propagation and critical flow rate in two-phase mixtures, J. Heat Transfer 111 (1989) 467–473.
[7] N.-N. Chung, W. Liu, Baushei Pei, A model for sound velocity in a two-phase air–water bubbly flow, Nucl. Technol. 99 (1992) 80–89.
[8] N.-N. Chung, W. Liu, B. Pei, A model for sound velocity and its relationship with interfacial area in a steam–water, two-phase bubbly flow, Nucl. Technol. 99 (1992) 258–267.
[9] V.J. Dejon, J. Firey, Effect of slip and phase change on sound velocity in steam–water mixtures and the relation to critical flow, I&EC Prog. Dev. 7 (3) (1968) 455–463.
[10] W.G. England, J.G. Firey, D.E. Trapp, Additional velocity of sound measurement in wet steam, I&EC Prog. Dev. 5 (2) (1966) 199–202.
[11] J. Weisman, T. Ake, R. Knott, Two-phase pressure drop across abrupt area changes in oscillatory flow, Nucl. Sci. Eng. 61 (1966) 297–309.
[12] J.J. Ginoux, Two-Phase Flow and Heat Transfer with Application to Nuclear Reactor Problems, Von Karman Institute for Fluid Dynamics, Rhode-Saint-Genese, Belgium, 1978.
[13] Rivkin, Aleksandrov, Kremenevskaya, Thermodynamic Derivations for Water and Steam, McGraw-Hill, New York, 1987.
[14] G.B. Wallis, One-Dimensional Two-Phase Flow, McGraw-Hill, New York, 1969.
[15] P. Griffith, G.A. Synder, The bubbly-slug transition in a high velocity two-phase flow, MIT report (1964) pp. 5003–5029.
[16] P. Griffith, G.B. Wallis, Two-phase slug flow, J. Heat Transfer 83 (1961) 307.
[17] K.H. Ardron, R.B. Duffey, Acoustic wave propagation in a flowing liquid–vapour mixture, Int. J. Multiphase Flow 4 (1978) 303–322.
[18] R.E. Henry, M.A. Grolmes, H.K. Fauske, Pressure pulse propagation in two-phase one and two component mixture, Argonne Natl. Lab. Rev. (1971) 7792.
[19] H.B. Karplus, Propagation of a pressure wave in a mixture of water and steam, Armour Res. Found. Illinois Institute Technol. Rep. (1961) 4132.
[20] Ozeitoun, M. Shoukri, V. Chatourgoon, Interfacial heat transfer between steam bubbles and subcooled water in vertical upward flow, J. Heat Transfer, ASW 117 (1995) 402–407.
[21] S. Kaizerman, E.E. Wacholder, Characteristics analysis of inhomogeneous, nonequilibrium, two-phase flows using the drift-flux model, Nucl. Sci. Eng. 84 (2) (1983) 168–173.